JOURNAL OF MATERIALS SCIENCE 19 (1984) 3487–3497

Factors influencing structural evolution in the oxide of hot-pressed Si_3N_4–Y_2O_3–SiO_2 materials

G. N. BABINI, A. BELLOSI, P. VINCENZINI
C.N.R., Research Institute for Ceramics Technology, Faenza, Italy

X-ray diffraction, SEM, EDS and WDS studies were performed of the structure and morphology of the oxide developed on hot-pressed compositions of the Si_3N_4–Si_2N_2O–$Y_2Si_2O_7$ sub-system subjected to short-term (~ 30 h) oxidation in air at $T = 1273$ to 1673 K. Viscosity of the oxide glassy phase, ionic mobility and oversaturation degree of the atomic species involved were found to be the most important parameters in the control of structural evolution of the oxide. Clear links appear to exist between compositional parameters of the grain-boundary phase of the hot-pressed materials and the evolution of the crystal phases in the oxide. The $\Sigma M_i/Y$ ratio (ΣM_i, total amount of metal impurities) in the grain-boundary phase, seems to play a major role in the transport properties of the oxide glassy phase.

1. Introduction

The parabolic oxidation of hot-pressed silicon nitride (HPSN) can be regarded in general as an internal oxidation driven by a surface reaction. A gradient in chemical potential is created between the silica produced at the oxide/sample interface and the intergranular phase, the governing mechanism possibly being associated with the migration of metal cations to the reaction interface to (i) minimize the free energy of mixing and (ii) reduce the total free energy by the reaction of Me^+ with SiO_2 and O^{2-} to form silicates at the surface. This suggests that a close link should exist between the composition and properties of the intergranular phase in HPSN and the composition, properties and structure of the oxide scale developed.

A diffusional model for the oxidation of Si_3N_4–Y_2O_3–SiO_2 hot-pressed materials, which is also useful for other dense nitrogen ceramics, has been developed previously [1, 2]; it proves useful in discussing both kinetic (oxidation rate constants K) and thermodynamic (apparent activation energy) aspects of the process. The amount of grain-boundary phase and concentration gradients of additive and metal impurities between the unreacted material and the silicon nitride/oxide reaction interface are the main parameters of the material introduced in the model.

The present paper summarizes the results of extended studies on the evolution of structure and morphology of the oxide developed on Si_3N_4–Y_2O_3–SiO_2 hot-pressed materials subjected to high temperature thermal treatment in air. These studies were finalized to gain more insight on phenomena occurring in the oxide scale and their relation to the characteristics of the grain-boundary phase.

2. Experimental details

Studies were performed on twelve compositions belonging to the Si_3N_4–Si_2N_2O–$Y_2Si_2O_7$ compatibility triangle of the Si_3N_4–Y_2O_3–SiO_2 system, where formation of high oxidizable yttrium oxinitrides is prevented [3]. They can be classified into three groups of approximately similar SiO_2/Y_2O_3 ratio (~ 2, ~ 3, ~ 5). In each group the Si_3N_4 content varies from ~ 72 to ~ 88 mol%. The notation xYz has been used in which $x = 1$ to 4 represents the Si_3N_4 content and $z = 2, 3, 5$ indicates approximately the SiO_2/Y_2O_3 ratio (Table I).

0022–2461/84 $03.00 + .12

TABLE I Compositions of the Si_3N_4–Y_2O_3–SiO_2 batches

		1Y2	2Y2	3Y2	4Y2	1Y3	2Y3	3Y3	4Y3	1Y5	2Y5	3Y5	4Y5
Si_3N_4	(mol%)	72.07	77.33	82.64	88.08	72.05	77.32	82.63	88.04	72.08	77.32	82.65	88.03
SiO_2	(mol%)	17.44	13.85	10.23	6.50	19.72	15.69	11.62	7.46	21.98	17.52	12.97	8.40
Y_2O_3	(mol%)	9.08	7.30	5.51	3.69	6.81	5.47	4.13	2.77	4.52	3.65	2.76	1.84
Impurities silic.	(mol%)	1.42	1.52	1.63	1.73	1.42	1.52	1.63	1.73	1.42	1.52	1.63	1.73
SiO_2/Y_2O_3 ratio	(mol%)	1.92	1.90	1.86	1.76	2.90	2.87	2.82	2.69	4.86	4.80	4.70	4.57

Hot-pressed samples were produced from batches of commercial Si_3N_4 powder* and reagent grade Y_2O_3 and SiO_2, mixed and homogenized for 72 h in a plastic jar with alumina balls in isobutyl alcohol, and subsequently dried, granulated and vacuum hot-pressed at 1973 K and 29.4 MPa in BN-lined graphite dies. The microstructure of the hot-pressed materials was studied by X-ray diffraction (XRD), scanning electron microscopy (SEM), and wavelength and energy dispersion system (WDS and EDS, respectively) microprobe analyses. Density was determined by geometrical and/or liquid displacement measurements.

Short-term (~ 30 h) oxidation experiments were carried out at $1173\,K \leqslant T \leqslant 1673\,K$ in 98 KPa air atmosphere on 10 mm × 10 mm × 2 mm polished and ultrasonically cleaned samples, diamond sawn from the hot-pressed billets. Weight gain was continuously recorded by using a TG apparatus capable of 2×10^{-5} g resolution. Heating and cooling rates were 20 and 10 K min^{-1}. Quenching experiments of oxidized samples to room temperature were also performed.

Surface and cross-sections of the oxide were analysed using XRD, SEM including BSE (back-scattering electron imaging), WDS and EDS. Parabolic weight gain curves were always observed. A detailed discussion of the kinetics and thermodynamics of the oxidation process is reported elsewhere [2].

3. Results

3.1. Phase composition of the hot-pressed materials

Fully $\alpha \rightarrow \beta$-Si_3N_4 converted materials resulted from 100 to 300 min hot-pressing, depending on composition. A typical SEM morphology (sample 3Y3 etched for 20 sec in molten NaOH) is shown in Fig. 1. SEM + EPMA analyses show that the impurities of the starting nitride powders (calcium, aluminium, iron etc.) segregate into the grain-boundary phase which X-ray diffraction shows to be composed of yttrialite (hydrogen, sodium, iron) $(Y, La)_5Si_6O_{21}$, miserite (calcium, potassium, sodium, aluminium, yttrium), SiO_3, δ- and α-$Y_2Si_2O_7$, Si_2N_2O and possibly $Y_5(SiO_4)_3N$ apatite whose amounts depend on sample composition.

A relevant fraction of the grain-boundary phase is frozen in a glassy state during cooling to room temperature. This partially devitrifies on further annealing. An X-ray semiquantitative evaluation of the approximate crystal phase content in the samples is given in Table II.

The presence of complex crystal phases such as miserite and yttrialite and of the glassy phase, together with the non-equilibrium conditions attained during hot-pressing, and the phase shift due to occurrence of a limited nitride volatilization at the hot-pressing temperature, prevent a precise

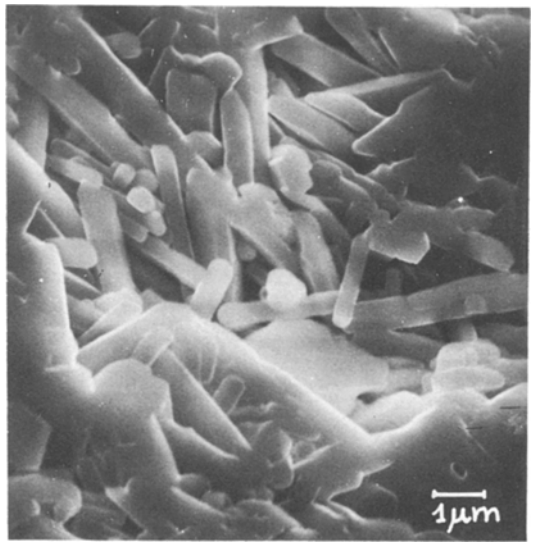

Figure 1 Scanning electron micrograph of a polished and etched surface of a 1Y3 sample hot-pressed at 1973 K and 29.4 MPa.

*Ame-Refractory Grade. BET specific surface area 3.72 $m^2\,g^{-1}$; amorphous SiO_2 1.9 wt%; Si (metal) 1.4 wt%; chemical analysis: Si (total) 58.41%; N 37.73%; Al 0.42%; Al 0.42%; Fe 0.46%; Ca 0.13%; Mg 220 ppm; K < 50 ppm; α/β ratio 3.8 (volumetric). Grain size (determined by TEM) 150 nm.

TABLE II Approximate XRD semiquantitative evaluation of the relative crystal phase content in the grain-boundary phase of hot-pressed Si_3N_4–Y_2O_3–SiO_2 compositions after annealing to 1573 K

	α-Si_3N_4	β-Si_3N_4	Si_2N_2O	ittrialite	miserite	δ-$Y_2Si_2O_7$	z-$Y_2Si_2O_7$	$Y_2O_3 \cdot 2SiO_2$
1Y2	–	71	–	17	5	1	1	5
2Y2	–	70	4	22	–	–	4	–
3Y2	–	77	–	–	–	–	–	23
4Y2	6	76	–	4	–	–	2	12
1Y3	–	67	15	13	tr	4	1	–
2Y3	–	68	11	13	2	2	–	4
3Y3	–	77	2	14	4	–	3	–
4Y3	9	70	8	6	–	–	2	7
1Y5	–	69	19	5	2	5	–	–
2Y5	–	73	15	9	–	–	3	–
3Y5	–	79	10	11	tr	–	–	–
4Y5	12	82	2	–	–	–	–	4

description of the grain-boundary phase on the basis of the ternary Si_3N_4–Y_2O_3–SiO_2 diagram. Nevertheless, by assuming specific reactions between Si_3N_4, Y_2O_3, SiO_2 and impurities [1, 2], the composition of the grain-boundary phase of the hot-pressed samples reported in Table III is obtained which has been shown [2] to represent adequately the real material, at least in terms of relative volumes of each constituent, in spite of the fact that the specific compounds used in the description are not exactly the same as those detected in the grain-boundary phase by X-ray diffraction.

3.2. Structure of the oxide

About fifteen different crystal phases have been detected in the oxide scale of Si_3N_4–Y_2O_3–SiO_2 hot-pressed materials, depending on sample composition and hot-pressing temperature. Among these, the more frequent and abundant are the following:

1. SiO_2 in the form of cristobalite, and occasionally of tridimite in samples oxidized at $T > \sim 1573$ K;

2. yttrium silicates, mainly yttrium disilicate (Y2S) and occasional yttrium meta-silicate;

3. magnesium and calcium silicates (akermanite and diopside) and magnesium silicates (enstatite and/or protoenstatite);

4. yttrialite and miserite.

Examples of the evolution of the content in the main crystal phases for samples of xY3 series derived from semiquantitative XRD* are reported in Figs. 2a to d, respectively. All other samples show approximately similar trends. The β-Si_3N_4 shown in Figs. 2a to d is that contained in the hot-pressed material; thus the Si_3N_4 curve in a first approximation reflects the trend in the increase in thickness of the oxide layer at increasing temperature.

The cristobalite content in the oxide always decreases with oxidation temperature up to

TABLE III Final compositions calculated according to Babini *et al.* [2] for the hot-pressed materials from the Si_3N_4–Y_2O_3–SiO_2 system obtained from batches in Table I.

		1Y2	2Y2	3Y2	4Y2	1Y3	2Y3	3Y3	4Y3	1Y5	2Y5	3Y5	4Y5
Si_3N_4	(mol %)	85.23	88.58	91.69	94.72	73.72	79.44	84.90	90.19	65.02	72.38	79.59	86.49
$Y_2O_3 \cdot 2SiO_2$	(mol %)	3.70	2.85	2.06	1.33	2.63	2.05	1.50	0.98	4.97	3.94	2.92	1.91
Si_2N_2O	(mol %)	5.64	3.94	2.35	0.76	19.38	14.76	10.33	6.02	28.45	22.05	15.77	9.80
Impurities	(mol %)	1.74	1.78	1.83	1.87	1.64	1.71	1.78	1.83	1.56	1.64	1.73	1.80
$2Y_2O_3 \cdot 3SiO_2$	(mol %)	3.70	2.85	2.06	1.33	2.63	2.05	1.50	0.98	–	–	–	–
Silicates (total)	(mol %)	9.14	7.48	5.95	4.53	6.90	5.81	4.78	3.79	6.33	5.58	4.65	3.71

*The simple relation: $I_i\% = I_i/\Sigma I_i$ has been used, where I_i is the height of maximum intensity diffraction of each phase with n being the number of crystal phases. No correction for preferred orientation effects was attempted.

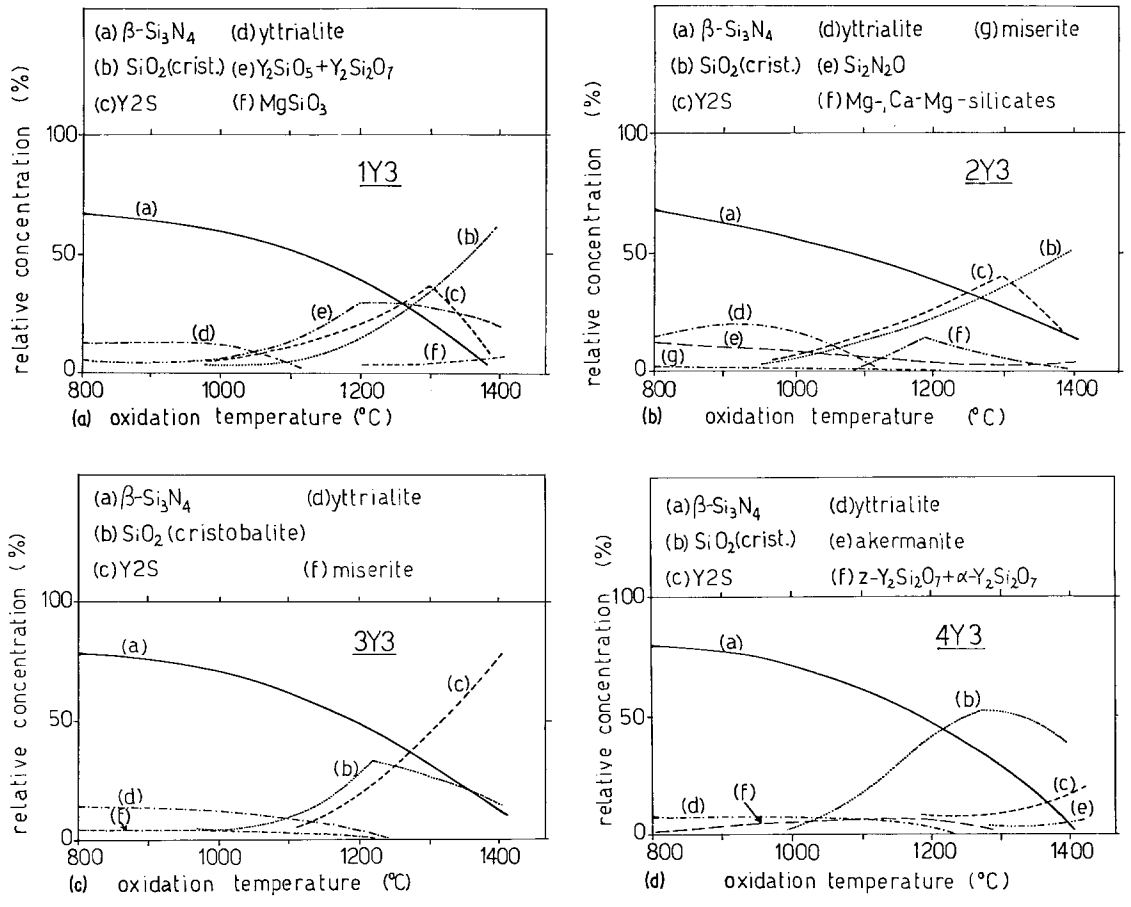

Figure 2 XRD evolution of crystal phases in sample xY3 after 30 h oxidation in air.

~ 1573 K. At $T > 1573$ K two apparently different trends are observed according to the preferred orientation degree of Y2S which aligns its (110), (220), (330) planes parallel to the oxide surface. Maximum intensity reflection is for the (220) plane; orientation increases with increasing oxidation temperature. SEM micrographs show that Y2S develops either needle-like and/or plate-like morphology in relation to the oxidation temperature, with their preferred growth directions coincident with those of preferred orientation.

For low Y2S orientation series 1Yx, 2Yx, cristobalite further increases in amount (see Figs. 2a and b); the reverse apparently occurs for samples 3Yx, 4Yx this being a possible consequence of the very strong texture of Y2S (Figs. 2c and d).

A comparison of cristobalite content in samples 1Y3 and 3Y3 oxidized at 1623 K and either quenched or slowly cooled to room temperature, shows that crystalline silica increases in amount by devitrification on cooling. The same tests indicate that the high-textured Y2S crystallizes at the oxidation temperature. Additional Y2S was found to devitrify on cooling, but in this case no appreciable preferred orientation is observed. Other forms of yttrium disilicate (δ-$Y_2Si_2O_7$, α-$Y_2Si_2O_7$, $Y_2Si_2O_7$ (thalenite), $Y_2Si_2O_7$ [4], of yttrium metasilicate Y_2SiO_5 [5–7] and of yttrium and calcium oxides ($Ca_3Y_2O_6$, CaY_4O_7) have occasionally been detected but always in scant amounts.

Magnesium and calcium silicates (akermanite and diopside) and magnesium silicates (enstatite and protoenstatite) are confined to 2Yx samples, mainly in limited amount and originated by devitrification on cooling.

Yttrialite and miserite belong to the grain-boundary phase of the hot-pressed materials. Their occasional presence in the oxide scale of materials oxidized at temperatures higher than

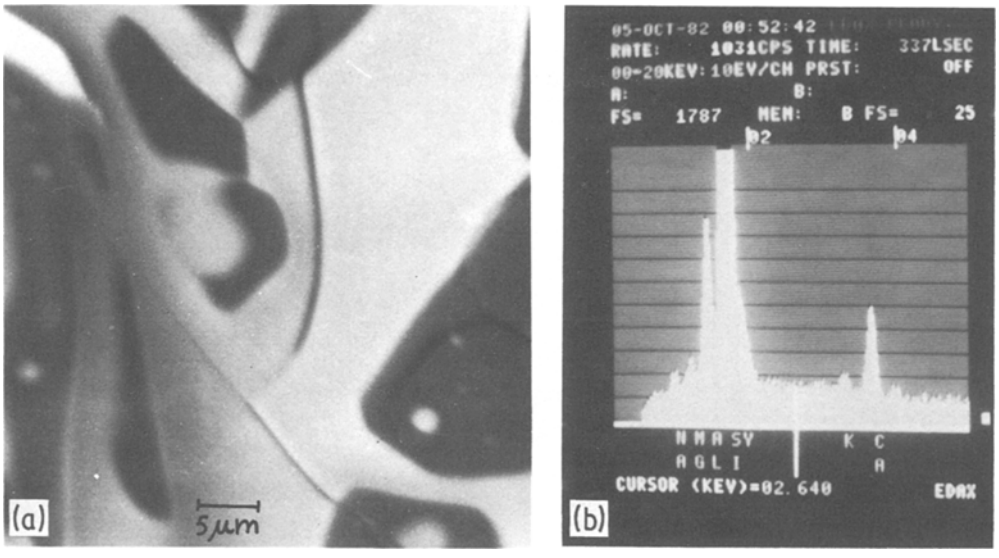

Figure 3 Sample 1Y3 oxidized 30 h at 1623 K: (a) BSE image of the oxide surface; (b) EDS of the glassy phase.

their stability field (~ 1273 K), might suggest that also these phases may undergo devitrification on cooling.

The residual glassy phase of the oxide is mainly composed of M_i (magnesium, calcium, aluminium, iron) and yttrium silicates (Fig. 3).

3.3. Morphology of the oxide

The variability of the morphology of the oxide scale on material composition and oxidation temperature is exemplified in Figs. 4a to g.

Selected micrographs and WDS maps showing the specific influence of the $\Sigma M_i/Y$ ratio on the morphology of oxide scale, for materials subjected to different oxidation and cooling conditions, are shown in Figs. 5a to m and Figs. 6a to d.

4. Discussion

The points considered below are based on a large number of experimental observations in the Si_3N_4–Y_2O_3–SiO_2 system of the effect of oxidation conditions and materials parameters, such as type and amount of grain-boundary phase, on the development of structure and morphology of the oxide, of which only few examples have been reported in Section 3. Discussion suffers limits inherent to scant knowledge of relationships between viscosity, ion mobility, degree of oversaturation in the oxide phase, and on temperature dependence of the above factors that are of utmost importance for oxidation.

Previous investigations [1, 2, 8, 9] indicate that the close link between the composition of the intergranular phase and the oxidation products is to be associated with the diffusion of the additive and metal cation impurities from the bulk of the material to its surface [10] in an attempt to equilibrate the chemical composition of the amorphous or glassy SiO_2 formed by oxidation of Si_3N_4 grains.

Thus the system can be qualitatively modelled as a composition of a "primary" (material) and a "secondary" (oxide) systems, ideally separated from each other by the reaction interface. The link is that the products of the "secondary" system form as a consequence of reactant species emerging from the "primary" system. Previous studies show that material transfer from the "primary" to the "secondary" system causes a continuous compositional change in the intergranular phase with formation of a gradient of depleted additive and impurity cations in the material [2, 8, 9].

The diffusional model formerly proposed [1, 2] for oxidation of Si_3N_4–Y_2O_3–SiO_2 hot-pressed materials accounts for the phenomena occurring in the "primary" system and at the Si_2N_4/oxide reaction interface. The main compositional factors of the "primary" system that were recognized to affect oxidation are the $Si_3N_4/(Y_2O_3 + SiO_2)$ and Y_2O_3/SiO_2 molar ratios, to which the total amount of intergranular phase and the concentration of silicates of yttrium and M_i are closely linked. The former is related

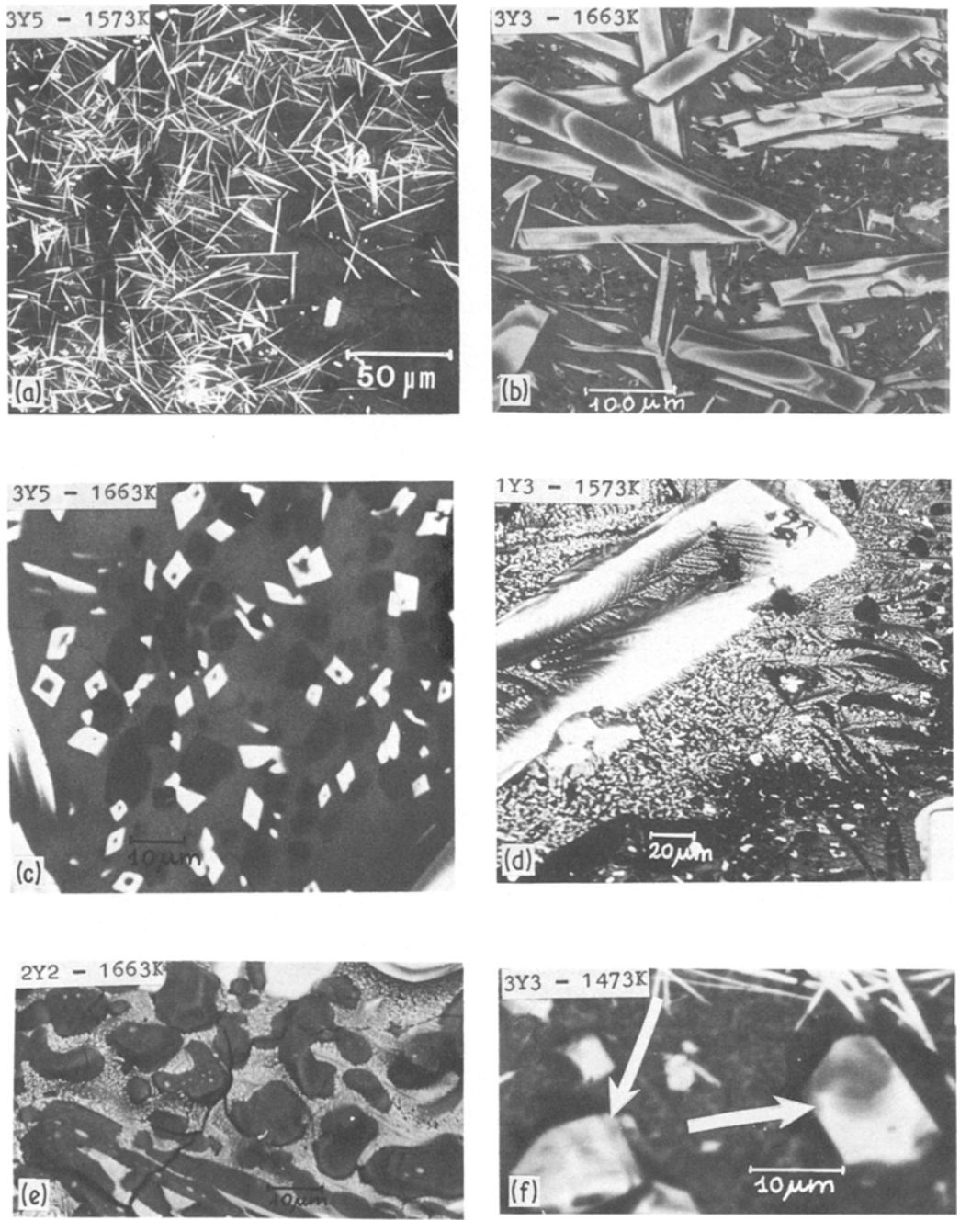

Figure 4 Scanning electron (BSE) micrographs of the surfaces of various compositions in the Si_3N_4–Y_2O_3–SiO_2 system oxidized in air for 30 h at various temperatures, showing the following morphologies: (a) needle-like Y2S; (b) plate-like Y2S; (c) rhombohedral Y2S; (d) dendritic Y2S; (e) cristobalite, dark areas; (f) arrows indicate granular miserite; (g) arrows indicate akermanite diopside.

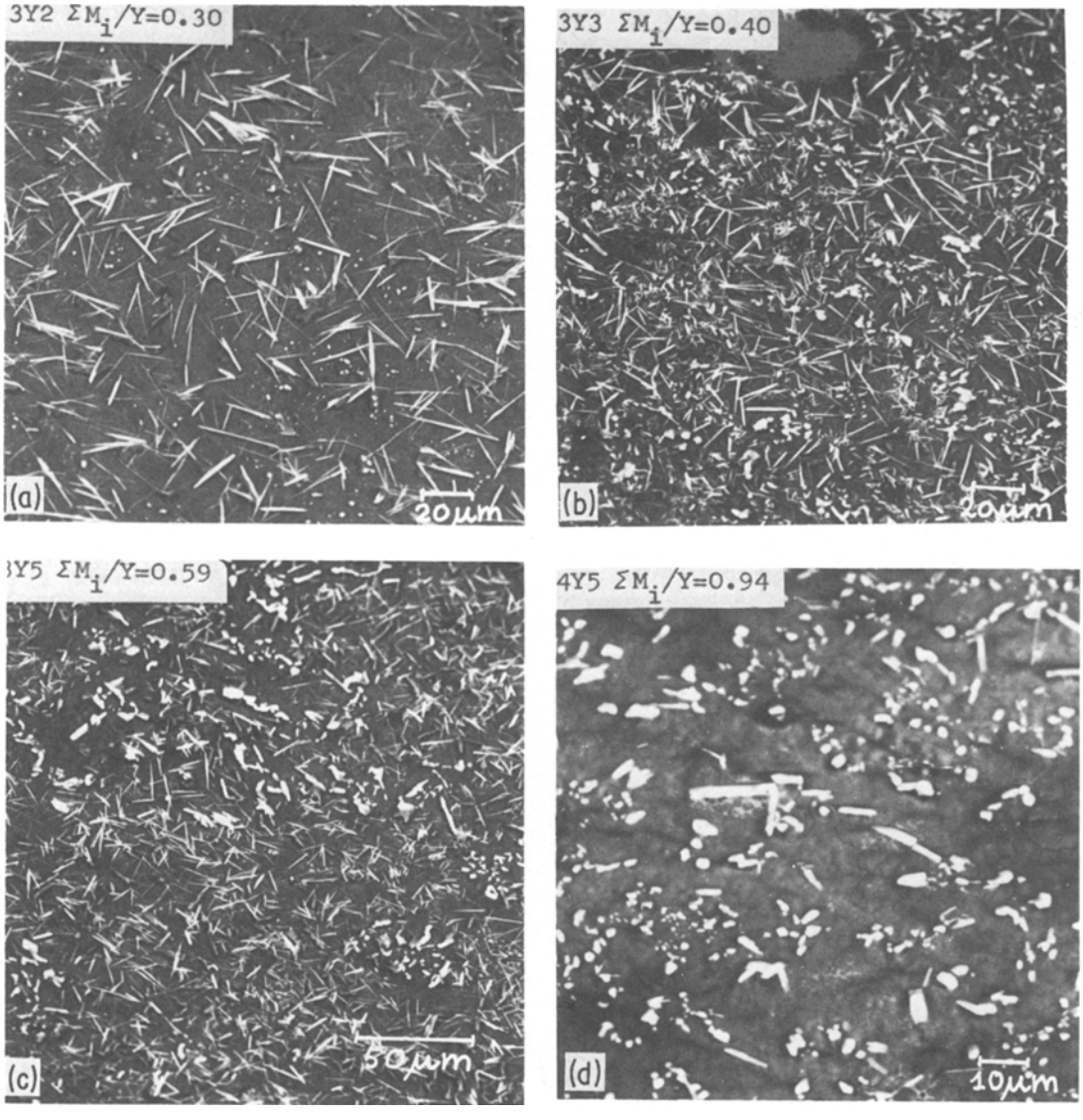

Figure 5 Scanning electron (BSE) micrographs of the surfaces of various compositions in the Si_3N_4–Y_2O_3–SiO_2 system oxidized for 30 h at different temperatures. (a) to (d) 1423 K. As a consequence of higher M_i mobility than Y, low Y oversaturation and high viscosity of the glassy phase, needle-like Y2S develops. For very high $\Sigma M_i/Y$ ratio, formation of miserite occurs preferentially. (e) to (h) 1573 K. Higher Y oversaturation and lower viscosity of the glass. Plate-like and needle-like morphologies compete in Y2S crystallization. At high $\Sigma M_i/Y$, miserite and needle-like Y2S develop. (i), (l) and (m) 1663 K. Very high Y oversaturation and lowest oxide phase viscosity. Y2S crystallization occurs along both the preferred growth directions and plate-like forms develop. Rhombohedral crystals detrify on cooling.

to the overall amount of material transferred to the Si_3N_4/oxide reaction interface; the latter determines the concentration gradient for outward diffusion of yttrium and M_i. The oxidation rate constant K is the experimental parameter which accounts for both factors.

The following general points can be derived from experimental data and from the model on the phenomena taking place in the "secondary" system of Si_3N_4–Y_2O_3–SiO_2 hot-pressed compositions:

1. the high silica glass produced as primary oxidation product is brought into chemical equilibrium with the intergranular phase of the hot-pressed material by the outward diffusion of yttrium and M_i cations, i.e. the situation existing in the "primary" system is reproduced and brought to further completion in the "secondary" system

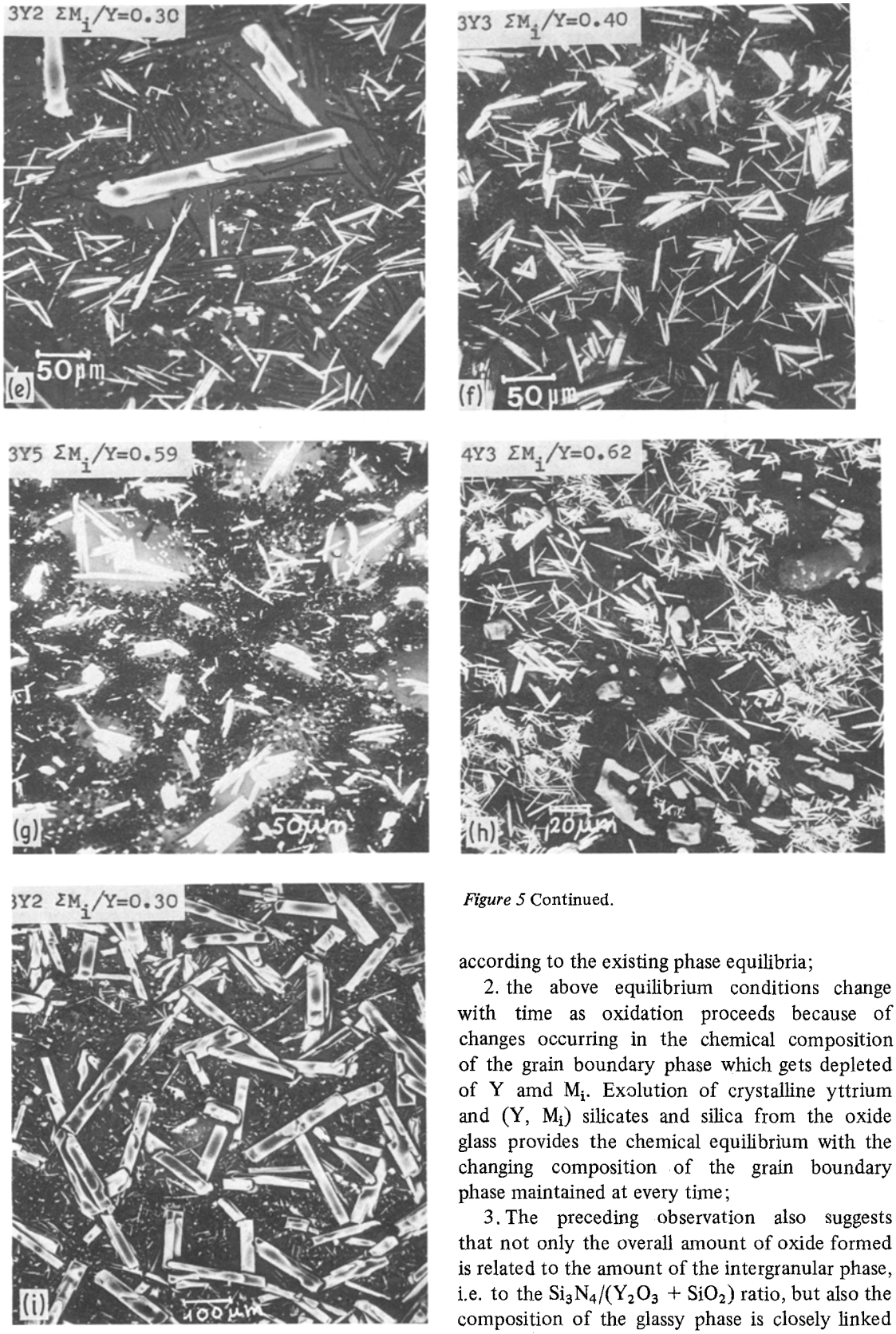

Figure 5 Continued.

according to the existing phase equilibria;

2. the above equilibrium conditions change with time as oxidation proceeds because of changes occurring in the chemical composition of the grain boundary phase which gets depleted of Y amd M_i. Exolution of crystalline yttrium and (Y, M_i) silicates and silica from the oxide glass provides the chemical equilibrium with the changing composition of the grain boundary phase maintained at every time;

3. The preceding observation also suggests that not only the overall amount of oxide formed is related to the amount of the intergranular phase, i.e. to the $Si_3N_4/(Y_2O_3 + SiO_2)$ ratio, but also the composition of the glassy phase is closely linked

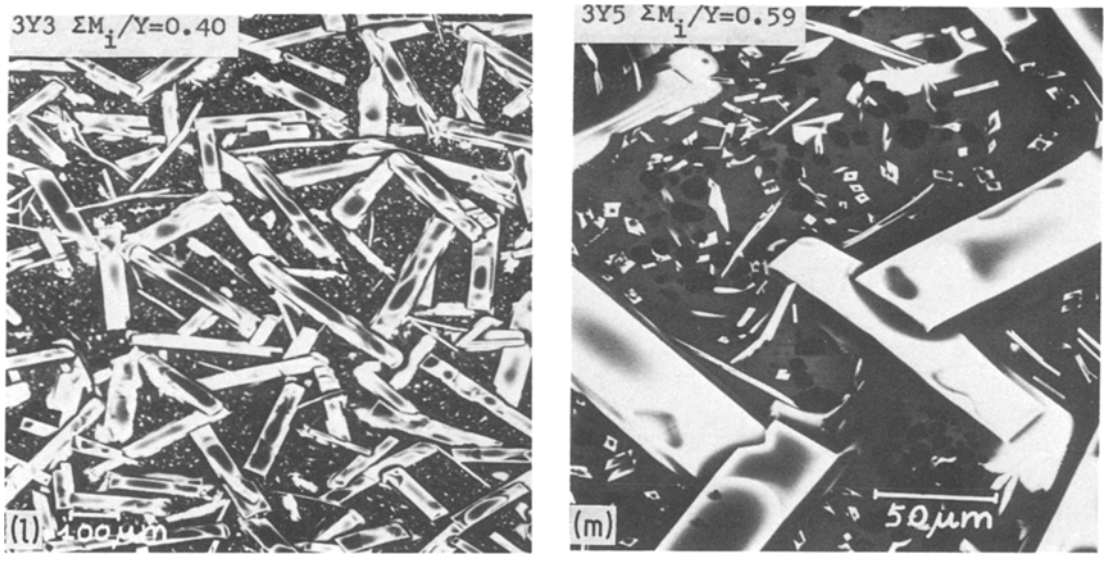

Figure 5 Continued.

to the Y_2O_3/SiO_2 and $\Sigma M_i/SiO_2$ in the intergranular phase. Both the ratios appear of significant importance as they affect the viscosity of the glassy phase, inherent ion mobilities and degree of oversaturation.

EDS semiquantitative analyses of the glass phase in the oxide scale of samples 1Y3 and 3Y3 fast quenched after 30 h oxidation at 1623 K (Figs. 6a to d) reported in Table IV show similarity between the $\Sigma M_i/Y$ ratios of 1Y3 to 3Y3 in the grain-boundary phase (~ 0.50) and that of the glassy phase in the oxide (~ 0.42), which is a direct experimental support to the above findings.

High concentrations of low melting point metal impurities (magnesium, aluminium, calcium, iron) in the intergranular phase results in a glassy oxide phase of relatively low viscosity which allows easy ion mobility and favours crystal phases of low solubility ions to exolute during the oxidation thermal treatment. High Y_2O_3 concentrations raise the liquidus temperature according to the Y_2O_3–SiO_2 phase diagram and, therefore, the viscosity at oxidation temperature. An approximate evaluation of the viscosity [11] of the oxide glassy phase for samples 1Y3 and 3Y3 results in values of 90 and 430 P, respectively, which agree with the previous deductions;

4. on cooling, conditions for further oversaturation can be realized causing nucleation and growth of new crystal phases or growth of preexistent crystals. Amount and morphology of devitrifying phases are related to the cooling rate;

5. solubility and mobility of yttrium and M_i cations in the viscous glassy phase are parameters which appear to determine the amount, type and morphology of the crystal phases in the oxide.

6. materials having the same chemical composition but differing in the amount of porosity behave similarly as regards the chemical composition of the oxide, the increase in "active" surface not involving changes in the transport properties of the reactants.

The crystallization behaviour of the Y2S phase in the oxide of the Si_3N_4–Y_2O_3–SiO_2 hot-pressed materials offers a chance to test the validity of the above concepts. Figs. 5 and 6 show that Y2S crystallizes in different morphologies related to oxidation temperature, material composition and cooling rate. XRD suggests the strongest preferred

TABLE IV EDS (at %) analysis of the chemical composition of the glass phase in the oxide of 1Y3 and 3Y3 samples oxidized at 1623 K for 30 h

Sample	1Y3	3Y3	$\frac{(\Sigma M_i/Y)_{1Y3}}{(\Sigma M_i/Y)_{3Y3}}$
Grain-boundary phase			
($\Sigma M_i/Y$)	0.20	0.40	0.50
Glassy phase in oxide			
Si (at %)	32	50	–
ΣM_i (at %)	20	25	–
Y (at %)	48	25	–
($\Sigma M_i/Y$)	0.42	1.00	0.42

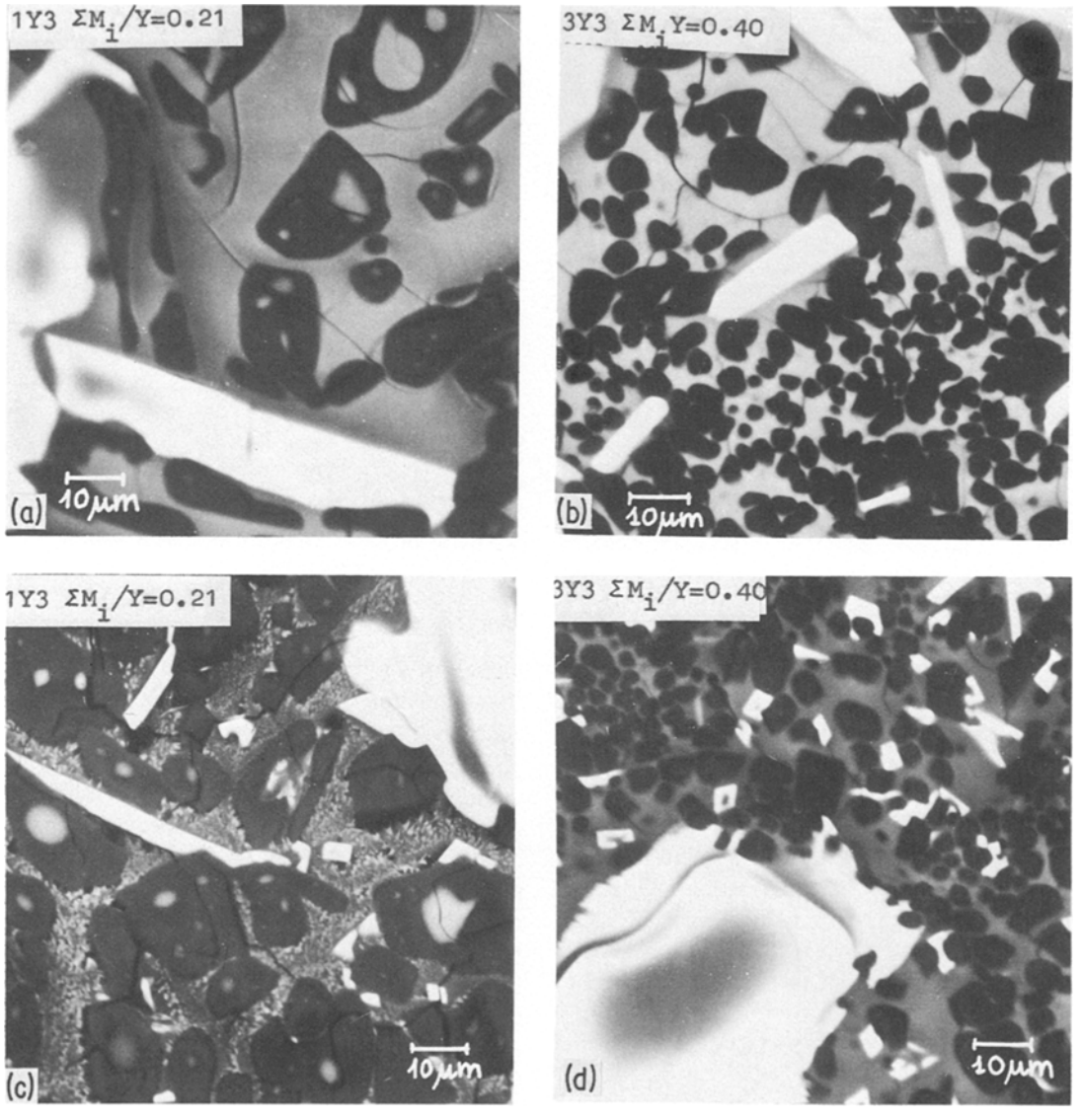

Figure 6 Scanning electron micrographs of the surface of samples of various compositions in the Si_3N_4–Y_2O_3–SiO_2 system subjected to different cooling rates after 30 h oxidation at 1623 K. (a) and (b) Quenching from 1623 K to room temperature. No devitrification occurs irrespective of the $\Sigma M_i/Y$ ratio. (c) and (d) Slow cooling from 1623 K to room temperature. Dendrites devitrify at low $\Sigma M_i/Y$; rhombohedral forms occur at high $\Sigma M_i/Y$.

orientation and growth directions of the Y2S along the (*hk*0) planes which align parallel to the oxide surface. Two energetic favoured crystallographic growth directions thus exist, one of which is most favoured. At low oxidation temperature, only high aspect ratio needle-like crystals develop (Figs. 5a to d), whereas the plate-like forms are the most preferred at higher oxidation temperatures (Figs. 5i, l and m); intermediate temperatures show both morphologies (Figs. 5e to h). Plate-like or needle-like forms of Y2S prevail at low and high $\Sigma M_i/Y$, respectively. Both forms develop during the oxidation run.

Other observations include:

1. the nucleation rate of high aspect ratio Y2S appears to increase at increasing $\Sigma M_i/Y$. For very high $\Sigma M_i/Y$, exolution of miserite is a strong competitor to Y2S crystallization (Figs. 5d and h);

2. Small rhombohedral and dendritic forms devitrify during slow cooling of samples subjected to the higher (~ 1663 K) oxidation temperatures

(Figs. 5m, 6c and d). A low $\Sigma M_i/Y$ ratio favours dendrites, whereas rhombohedral forms are typical of high $\Sigma M_i/Y$ ratios. These forms were never observed in samples fast quenched to room temperature (Figs. 6a and b) irrespective of the $\Sigma M_i/Y$ ratio.

The previous observations can be tentatively explained on the basis of the general rules of crystal growth from oversaturated melts:

1. the lower the oxidation temperature, the higher is the $\Sigma M_i/Y$ ratio in the oxide glass due to the higher diffusion coefficient in the intergranular phase of M_i cations as compared with yttrium. Because of the high viscosity of the oxide glass due to the relatively low oxidation temperature, the low oversaturation degree of yttrium and its relatively low mobility, the formation of Y2S occurs along with the most energetically favoured direction. Therefore, needle-like crystals form;

2. the higher the oxidation temperature, the lower the $\Sigma M_i/Y$ ratio in the oxide glass as a consequence of the higher "apparent" activation energy for diffusion in the intergranular phase of yttrium compared to M_i [9, 10]. Owing to the high degree of oversaturation of yttrium and its relatively high ionic mobility as a consequence of the lower viscosity of the glassy oxide phase, crystallization of Y2S occurs along with both the preferred growth directions, and plate-like Y2S develops;

3. viscosity of the oxide glassy phase, oversaturation degree of yttrium and its mobility are the main parameters which account also for the "habitus" of Y2S devitrified on cooling. Both rhombohedral and dendritic forms result from a slow cooling rate. Formation of dendrites occurs more easily in a relatively viscous and strongly Y oversaturated glass (sample 1Y3, $\Sigma M_i/Y = 0.21$, Fig. 6c), whereas rhombohedral forms are favoured if Y oversaturation is less pronounced and the glass is less viscous (sample 3Y3, $\Sigma M_i/Y = 0.40$, Fig. 6d). As a possible consequence of local chemical inhomogeneity of the glassy oxide, conditions are also met in which the simultaneous exolution of dendritic and rhombohedral Y2S occurs.

5. Conclusions

At given oxidation conditions, the main material parameters which affect the structure and morphology of the oxide formed on dense hot-pressed Si_3N_4–Y_2O_3–SiO_2 compositions, i.e. viscosity of the glassy oxide phase, ionic mobility and oversaturation degree of the reactant species are closely related to the experimental oxidation rate constants. The latter, in turn, account for the main characteristics of the intergranular phase in the hot-pressed material such as its amount, composition, transport properties and related concentrational gradients which are established between bulk and Si_3N_4/oxide reaction interface. Thermochemical equilibrium between the intergranular phase ("primary" system) and the oxide phase ("secondary" system) is realized by the outward diffusion of metal cations to the Si_3N_4/oxide reaction interface where they combine with the silica deriving from oxidation of Si_3N_4 grains. The general trend of the oxide is to evolve to rebuild the grain-boundary phase composition, with reactions proceeding to approach equilibrium conditions.

The morphology of yttrium disilicate crystallized in the oxide phase has been explained in terms of the effect of oxidation temperature, compositional parameters and quenching rate. Among compositional parameters, the role of $\Sigma M_i/Y$ ratio appears crucial.

References

1. G. N. BABINI and P. VINCENZINI, Oxidation of hot pressed silicon nitride, in "Progress in Nitrogen Ceramics", edited by F. L. Riley, NATO: ASI Series, Series Z Applied Science n. 65 (Martinus Nijhoff, 1983) pp. 427–38.
2. G. N. BABINI, A. BELLOSI and P. VINCENZINI, *J. Mater. Sci.* **19** (1984) 1029.
3. F. F. LANGE, S. C. SINGHAL and R. C. KUZNICKI, *J. Amer. Ceram. Soc.* **60** (1977) 249.
4. J. C. P. D. S. (International Center for Diffraction Data) Powder Diffraction File 20-1416.
5. J. C. P. D. S. (International Center for Diffraction Data) Powder Diffraction File 22-992.
6. J. C. P.D. S. (International Center for Diffraction Data) Powder Diffraction File 21-1456.
7. J C. P. D. S. (International Center for Diffraction Data) Powder Diffraction File 21-1458.
8. S. C. SINGHAL, Oxidation of silicon nitride and related materials, in "Nitrogen Ceramics", edited by F. L. Riley, NATO: ASI Series, Series E Applied Science n. 23 (Noordhoff, Leiden, 1977) pp. 607–24.
9. G. N. BABINI, A. BELLOSI and P. VINCENZINI, *J. Mater. Sci.* **18** (1983) 231.
10. *Idem, J. Amer. Ceram. Soc.* **64** (1981).
11. G. URBAIN, F. CAMBIER, M. DELETTER and M. R. ANSEAU, *Trans. J. Brit. Ceram. Soc.* **80** (1981) 139.

Received 10 October
and accepted 19 December 1983